Supplementary Information for

Vibrational Dynamics of Oxygenated Heme Proteins

Weiqiao Zeng[a], Alexander Barabanschikov[a], Ningyan Wang[b], Yi Lu[b], Jiyong Zhao[c], Wolfgang Sturhahn[c], E. Ercan Alp[c], and J. Timothy Sage[a]
[a]Department of Physics and Center for Interdisciplinary Research on Complex Systems, Northeastern University, Boston, Massachusetts, USA 02115
[b]Department of Chemistry, University of Illinois at Urbana Champaign, Illinois, USA 61801
[c]Advanced Photon Source, Argonne National Laboratory, Argonne, Illinois, USA 60439

1 Methods

Preparation of Isotopically Enriched MbO_2: ^{57}Fe labeled myoglobin was obtained through reconstitution of native horse heart myoglobin (Sigma) following published procedures [1–3]. Briefly, the hemes were first extracted by mixing 2-butanone with a solution of the protein at pH 1.0 and 4 °C and allowing the aqueous and organic phases to separate [1]. Following sequential dialysis of the resulting apoprotein solution against 0.01 M $NaHCO_3$ and 0.01 M potassium phosphate, pH 7.0 [3], addition of ^{57}Fe(III) or ^{54}Fe(III) protoporphyrin IX chloride [Fe(PPIX)(Cl)] (Frontier Scientific, Logan, UT) at pH 8.0-9.0 (dissolved in 0.1 M NaOH) at 4 °C led to reconstitution of the holoprotein. The reconstituted proteins were purified by removing aggregated proteins through centrifugation and then separating extra hemes on an ion exchange gel column (Sephadex CM C-50, Sigma) at pH 7.0 [3]. The product was then stirred overnight to allow equilibration of the heme-protein complex. Raman spectra of native and reconstituted proteins exhibit excellent agreement (Fig. S2), particularly in the $350-430$ cm^{-1} region, which contains propionate and vinyl bending modes that are highly sensitive to heme orientation [4], confirming that heme rotational equlibrium has been established.

MbO_2 was prepared by reducing myoglobin with excess sodium dithionite, then passing through a size exclusion gel column (Sephadex G-25, Sigma) equilibrated with 0.1 M pH 8 potassium phosphate buffer. A ^{57}Fe-enriched sample was centrifuged to a final concentration of approximately 13 mM, and loaded into the NRVS sample cell. For Raman measurements, MbO_2 solutions (native or reconstituted) were prepared at $1-2$ mM concentration and frozen on nylon cryoloops (Hampton Research).

Preparation of Isotopically Enriched Cu_BMb: Cu_BMb was expressed and purified as described in [5]. Reconstitution with ^{57}Fe(PPIX)(Cl) followed procedures similar to horse Mb except that excess heme was removed by passage through a PD10 size exclusion column (Amersham Bioscience) [6]. Reconstituted Cu_BMb in 0.02 M Mops pH 8 was reduced by dithionite and passed through a size-exclusion column to remove excess reductant before adding five equivalents of $AgNO_3$. Electronic absorption (Fig. S6) confirmed formation of the Ag(I)$-Cu_B MbO_2$ complex. The resulting protein was concentrated to a minimum volume ($\sim$ 8 mM). About 80 μL concentrated solution was loaded into a NRVS sample cell. Following NRVS data collection, Raman data were recorded using the same sample cell. All protein samples for NRVS measurements were stored and transported to and from the beamline in a dry shipper precooled with liquid nitrogen.

Raman Measurement: Cryogenic resonance Raman spectra were recorded using a confocal Raman microscope (LabRam HR800, Horiba JY). Scattering was excited using the 413.1 nm line of a krypton laser (Innova 302C, Coherent). Average power density on the sample was controlled by attenuating beam power, and, for MbO_2, by continuously scanning the laser spot ($\approx 20\,\mu m$ in diameter) along a line during data collection. The primary frequency calibration, based on the 520.7 cm^{-1} line of silicon, was confirmed using Raman scattering from fenchone [7]. The resolution of the Raman spectra is 2 cm^{-1}. For MbO_2,

scattered light was collected from freestanding films frozen on nylon cryoloops and maintained at cryogenic temperature in a 100 K nitrogen stream from a commercial cryocooler (Oxford Cryosystems), using 1.8 mW beam power. Raman scattering from the Ag(I)−$Cu_B$$MbO_2$ NRVS sample, mounted in a helium cryostat (MicrostatHe, Oxford Instruments), was excited and collected directly through a sapphire window at the back of the sample cell using 0.5 mW beam power.

The observation of similar frequencies for the structural markers ν_4, ν_2, and ν_{10} (Fig. S7) confirms that heme coordination is unaltered in the presence of the Ag(I) ion. Appearance of a second ν_4 band at 1356 cm^{-1} indicates significant O_2 photolysis for MbO_2, while very little photolysis is evident for Ag(I)-MbO_2.

Fig. S8 reveals numerous frequency and intensity differences at lower frequencies. Many of the observed vibrations have frequencies similar to MbCO, where isotope labelling of the heme has suggested assignment to porphyrin vibrations [8]. However, improved spectral resolution at 100 K reveals multiple contributions to features that appear to be single bands in room temperature measurements (Fig. S8).

NRVS Data Collection and Analysis: Nuclear resonance vibrational spectroscopy (NRVS) data were collected at sector 3-ID-D of the Advanced Photon Source at Argonne National Laboratory, as described in detail elsewhere [9, 10]. Briefly, extremely relativistic electron bunches passing through an undulator inserted in the storage ring generated X-ray pulses. A high heat-load monochromator reduced the X-ray bandwidth to about 1 eV, centered at the 14.4125 keV nuclear resonance energy of the Mössbauer isotope ^{57}Fe, and was followed by a high resolution monochromator [11] that further reduced the bandwidth to 1.2 meV (≈10 cm^{-1}). The X-ray beam was highly collimated, with a cross section of about 0.5×0.5 mm^2 at the sample position. The high resolution monochromator scanned the energy of the X-ray beam incident on the sample in the vicinity of 14.4125 keV with a step size of 0.25 meV. At each point, signal was counted for 5 seconds. The incident 14.4125 keV X-ray flux was approximately 10^9 Hz. The scanning range of energy is from -30 to +80 meV to include all possible significant Fe modes.

An avalanche photodiode detector (APD) detected X-rays emitted from the sample. Timing circuitry excluded prompt events coincident with the X-ray pulse, due to scattered photons, and counted events delayed in time with respect to the incident X-ray pulse, which are emitted by excited ^{57}Fe atoms. The resulting delayed count rate monitors ^{57}Fe absorption as a function of incident X-ray energy. Approximately 15 energy scans (40-50 minutes each) were collected and averaged for each sample, and comparison of initial and final scans confirmed the absence of spectroscopic changes due to radiation damage.

The measured NRVS data were processed with the program PHOENIX [12]. In general, individual scans were summed and then normalized to the recoil energy E_R = 1.96 meV of a free ^{57}Fe nucleus, according to Lipkin's sum rule, [13] $\int_{-\infty}^{\infty} ES(E)\,dE = E_R$, to yield the excitation probability $S(E)$. PHOENIX extracted the Fe-weighted vibrational density of states (Fe VDOS) $D(E)$ from $S(E)$ by removing the recoilless peak at $E = E_0$, multiphonon contributions and temperature dependence [12, 14]. An 11% contribution from oxidized Mb to the NRVS signal for horse MbO_2, estimated from the absorption spectrum (Fig. S9), was removed manually during data processing. The input sample temperature is adjusted to be consistent with the ratio of Stokes and anti-Stokes contributions to $S(E)$. For convenient comparison with Raman spectra, the VDOS is presented as a function of the frequency $\bar{\nu} = (E - E_0)/hc$, with $D(\bar{\nu})$ rescaled to maintain the normalization

$$\int D(\bar{\nu})\,\mathrm{d}\bar{\nu} = 3. \tag{S1}$$

Fig. 2 in the main text presents the VDOS as data points with gray error bars, together with solid curves representing 5-point running averages.

The energy scale of NRVS data was adjusted by less than 2%, based on comparison with an established calibration standard. The MbO_2 calibration used the reported ν_4 frequency of $K_2Mg\,^{57}Fe(CN)_6$ [15], and was confirmed by coincidence of the 579 cm^{-1} frequency with the independently calibrated Raman frequency. The Ag(I)−$Cu_B$$MbO_2$ energy scale was established by Raman measurements of the O_b-centered FeOO vibration at 588 cm^{-1}.

The stiffness [16–18]

$$k_s = m_{\mathrm{Fe}}\langle\omega^2\rangle = m_{\mathrm{Fe}}(2\pi c)^2\frac{1}{3}\int D(\bar{\nu})\bar{\nu}^2\,\mathrm{d}\bar{\nu} \tag{S2}$$

determined from the VDOS measures the average strength of nearest neighbor bonds to the iron. The stiffness is sensitive to the measurement of background and resolution function, which are inputs in the PHOENIX program to generate VDOS. An appropriate background can be determined by averaging the high energy end of the NRVS data where no iron vibrations appear. The resolution function should also be measured at the same X-ray beam configuration as the NRVS data collection on protein samples.

For both compounds, the stiffness, an averaged force constant measuring Fe-ligand bond strength [16–18], has a 370 pN/pm value, at the upper end of the range associated with previous measurements of low spin heme Fe, and significantly higher than the 170 – 250 pN/pm values reported for high spin compounds (Table S2).

2 Computational Methods

DFT calculations were performed with Gaussian 03 [19] using the B3LYP functional [20,21]. The basis set was Ahlrichs VTZ [22] for the Fe atom and 6-31G* for all other atoms. Vibrational calculations specified the ^{57}Fe isotope for the heme iron and used default masses for all other atoms. Previous results have shown the necessity of including peripheral groups in the calculation to obtain accurate modelling of heme vibrations [23,24]. In addition, our model for the MbO_2 active site, shown in Fig. S3, constrained the orientation of the His 64 imidazole ring by incorporating a hydrogen bonding network involving Ser92 and one of the heme propionates. In spite of this, the calculation yielded one imaginary frequency corresponding to torsion around the Fe-N_{Im} bond to His 64. An ammonia replaces the Arg45 residue that forms a hydrogen bond to the second heme propionate in the protein.

Table S3 compares selected geometric parameters of the optimized structure. The closed-shell electronic configuration resulting from the present spin-restricted calculation predicts an Fe-O bond slightly shorter than found in crystallographic models, in agreement with previous results. [25, 26] Previous unrestricted calculations yielded open-shell configurations that have lower energy but predict Fe-O bonds longer than observed [25,26]. Agreement is generally better for other structural parameters (Table S3), and the closed-shell calculation provides adequate guidance for interpreting the vibrational observations.

Vibrational calculations yield the VDOS for each atom in the molecule. The VDOS for the Fe and the two atoms of the dioxygen ligand describe the predicted kinetic energy distribution over the FeOO fragment (Figs. S4, S5). For the Fe atom, the predicted VDOS can be compared directly with the experimental VDOS on an absolute scale, as shown in Fig. 2 of the main text.

The partial VDOS [27]

$$D_j^{\hat{k}}(\bar{\nu}) = \sum_{\alpha}\left(\hat{k}\cdot\vec{e}_{j\alpha}\right)^2\mathcal{L}(\bar{\nu}-\bar{\nu}_\alpha) \tag{S3}$$

along direction $\hat{k}$ (for oriented samples) includes contributions at the frequency of each vibrational mode $\bar{\nu}_\alpha$, weighted by the vibrational displacement of atom j along the direction of the X-ray beam. Here, $\mathcal{L}(\bar{\nu}-\bar{\nu}_\alpha)$ is a normalized line shape function. To facilitate comparison with the experimental VDOS in Fig. 2 of the main text, we choose a Gaussian lineshape with full width at half maximum Γ=16 cm^{-1} for $\mathcal{L}(\bar{\nu}-\bar{\nu}_\alpha)$.

Since the mode composition factor $e^2_{j\alpha}$ is the fraction of kinetic vibrational energy of the molecule on atom j for mode $\bar{\nu}_\alpha$ [27], we calculate the vector

$$\vec{e}_{j\alpha} = \sqrt{m_j}\frac{\partial\vec{r}_j}{\partial Q_\alpha} = \frac{\sqrt{m_j}\,\vec{r}_j}{\sqrt{\sum m_j r_j^2}} \tag{S4}$$

and its squared value

$$e_{j\alpha}^2 = \frac{m_j\, r_j^2}{\sum m_j r_j^2} \tag{S5}$$

from the masses m_j and predicted vibrational displacements $\vec{r}_j$ of atom j [23]. The VDOS

$$D_j(\bar{\nu}) = \sum_\alpha e_{j\alpha}^2 \mathcal{L}(\bar{\nu} - \bar{\nu}_\alpha) \tag{S6}$$

is summed over the three directions for comparison with experimental data recorded on randomly oriented samples. Six modes corresponding to molecular rotation and translation appear at zero frequency in the calculation on an isolated molecule and are omitted from the summations in Eqn. (S3) and (S6). The predicted stiffness (k_s) can be calculated by inserting $D_j(\bar{\nu})$ into Eqn. (S2).

Since $\vec{r}_j$=(x, y, z), we can also obtain the squared value of $\vec{e}_{j\alpha}$ and vibrational density of states along each axis direction,

$$e_{j\alpha,x}^2 = \frac{m_j\, x_j^2}{\sum m_j r_j^2},\ D_{j,x}(\bar{\nu}) = \sum_\alpha e_{j\alpha,x}^2 \mathcal{L}(\bar{\nu} - \bar{\nu}_\alpha) \tag{S7}$$

$$e_{j\alpha,y}^2 = \frac{m_j\, y_j^2}{\sum m_j r_j^2},\ D_{j,y}(\bar{\nu}) = \sum_\alpha e_{j\alpha,y}^2 \mathcal{L}(\bar{\nu} - \bar{\nu}_\alpha) \tag{S8}$$

$$e_{j\alpha,z}^2 = \frac{m_j\, z_j^2}{\sum m_j r_j^2},\ D_{j,z}(\bar{\nu}) = \sum_\alpha e_{j\alpha,z}^2 \mathcal{L}(\bar{\nu} - \bar{\nu}_\alpha). \tag{S9}$$

Guided by measurements of vibrational anisotropy in nitrosyl porphyrins [28], we choose a coordinate system such that the x-axis lies along the intersection of the FeOO plane and the mean plane of the four pyrrole nitrogen atoms, the y-axis is normal to the FeOO plane and the z-axis is normal to the mean porphyrin plane.

3 Relating Isotope Shifts and VDOS Areas

In the normalized VDOS for atom j (Eq. S6), each mode contributes an area equal to the mode composition factor $e_{j\alpha}^2$ [27]. Thus, curve fitting to the Fe VDOS quantifies the mean squared amplitude (proportional to $e_{j\alpha}^2$) as well as the frequency of the Fe motion.

Mass perturbations resulting from isotope substitution can provide similar information, if they are small enough to shift frequencies without changes in mode character due to vibrational mixing. In the limit of small mass changes, the frequency shift $\Delta\bar{\nu}_\alpha$ of mode α in response to a change Δm_j in the mass of atom j determines the mode composition factor [27]

$$e_{j\alpha}^2 = -2\frac{d(\ln \bar{\nu}_\alpha)}{d(\ln m_j)} \approx -2\frac{\Delta\bar{\nu}_a/\bar{\nu}_a}{\Delta m_j/m_j}. \tag{S10}$$

4 Supplementary Tables and Figures

Table S1: Vibrational frequencies of the FeOO fragment in O_2 complexes of heme proteins and porphyrins[a]

		FeOO frequency (cm^{-1})		
protein	temperature	Fe-centered	O_b-centered	reference
Ag(I)–Cu_BMb[b]	95 K	428	588	this work
Mb[b]	73 K	423	579	this work
Fe(TpivPP)(2-MeIm)[b]	25 K	419/389	563	[26]
Fe(TpivPP)(1-MeIm)[b]	25 K	417/393	571	[26]
Mb[b]	ambient	–	572	this work
Mb	ambient	–	571	[29]
cytochrome *c* oxidase	ambient	435	571	[29]
human HbA	ambient	425	568	[29, 30]
heme oxygenase	ambient	414	565	[31]
Mb L29W	ambient	–	574	[32]
Mb H64L	ambient	–	570	[32]
Mb L29F	ambient	–	568	[32]
dehaloperoxidase	ambient	–	571	[33]
cyt *c′* L16A	ambient	–	572	[34]
indoleamine dioxygenase	ambient	–	569	[35]
FixLH	ambient	–	569	[36]
Tt H-NOX	ambient	–	567	[37]
cyt b_5 H39V	ambient	–	566	[38]
DevS	ambient	–	563	[39]
Paramecium Hb	ambient	–	563	[40]
EcDos	ambient	–	562	[36]
HemAT	ambient	–	560	[41]
Mycobacterium trHbN	ambient	–	560	[42]
Mycobacterium trHbO	ambient	–	559	[43]
Chlamydomonas Hb	ambient	–	554	[44]
Synechocystis Hb	ambient	–	554	[44]
Campylobacter trHbP	ambient	–	542	[45]
cytochrome $P450_{cam}$	ambient	402	540	[46]
cobalt-substituted Hb	ambient	390	537	[47]
nitric oxide synthase	ambient	–	517	[48]

a Abbreviations: Mb, myoglobin; Hb,hemoglobin; trHb, truncated hemoglobin *b* Heme enriched with ^{57}Fe.

Table S2: Stiffness values determined from experimental VDOS for heme proteins measure the average strength of Fe ligation.

protein	spin	axial ligands		stiffness (pN/pm)	ref
Ag(I)-$Cu_B$$MbO_2$	0	His93	O_2	373 ± 13	this work
MbO_2	0	His93	O_2	371 ± 9	this work
MbNO	1/2	His93	NO	368 ± 10	[49]
Fe(II) cyt *c*	0	His18	Met 80	322 ± 17	[18]
Fe(III) cyt *c*	1/2	His18	Met 80	284 ± 17	[18]
Fe(II) cyt *f*	0	His25	N-terminus	342 ± 18	[17]
Fe(III) cyt *f*	1/2	His25	N-terminus	313 ± 34	[17]
deoxyMb	2	His93	–	190 ± 20	[18]
metMb	5/2	His93	H_2O	235 ± 4	this work
MbO_2 model	0	His93	H_2O	446	this work

Table S3: Selected geometric parameters of the optimized MbO_2 model structure shown in Fig. S3, in comparison with crystallographic structural models.

parameter	computational model	crystallographic model	
		PDB:2Z6S [50]	PDB:1A6M [51]
$Fe-O_b$	176.5 pm	182.6 pm	180.6 pm
O_b-O_t	127.1 pm	124.9 pm	123.5 pm
$\angle FeO_bO_t$	122.0°	124.2°	122.5°
$Fe-N_1$	203.1 pm	198.9 pm	200.1 pm
$Fe-N_2$	202.0 pm	200.8 pm	199.7 pm
$Fe-N_3$	201.7 pm	195.1 pm	200.3 pm
$Fe-N_4$	202.5 pm	198.0 pm	202.3 pm
$Fe-N_{Im}$	208.0 pm	208.4 pm	206.4 pm

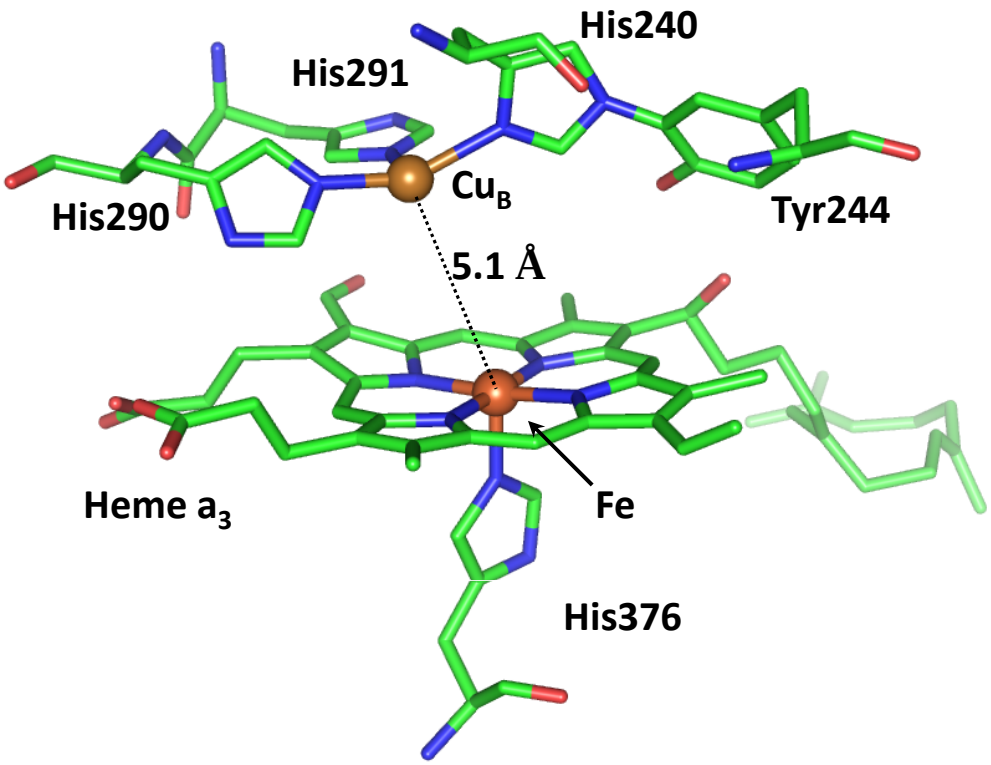

Figure S1: Crystallographic structural model for the catalytic site of bovine cytochrome *c* oxidase (PDB code: 2OCC), showing three histidines coordinating a Cu 5 Å from the Fe of heme a_3 that binds the O_2 substrate. Cu_BMb [52] models this site by engineering a second metal binding site into Mb.

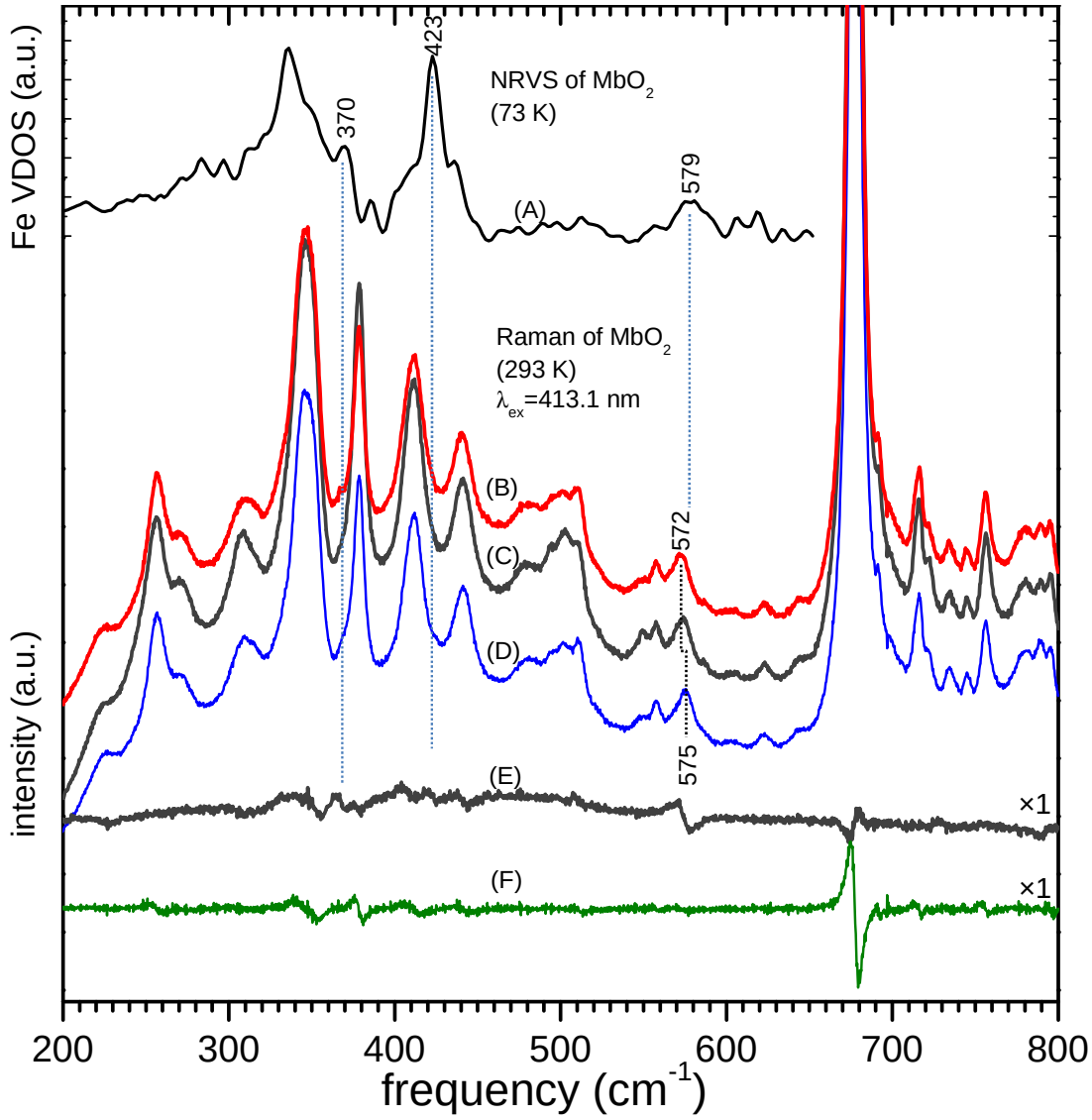

Figure S2: Vibrational data recorded on horse MbO_2 confirm successful reconstitution with isotopically enriched heme and reveal contributions from Fe motion. Trace A is the Fe VDOS determined at 100 K using NRVS, for comparison with Raman spectra recorded at ambient temperature: trace B:^{57}Fe-enriched MbO_2, trace C: native MbO_2, trace D: ^{54}Fe-enriched MbO_2, trace E: difference between B and D. Trace F is obtained by shifting trace B to lower frequency by 0.3 cm^{-1} and subtracting the original spectrum, providing a reference that excludes significant grating drift. [31].

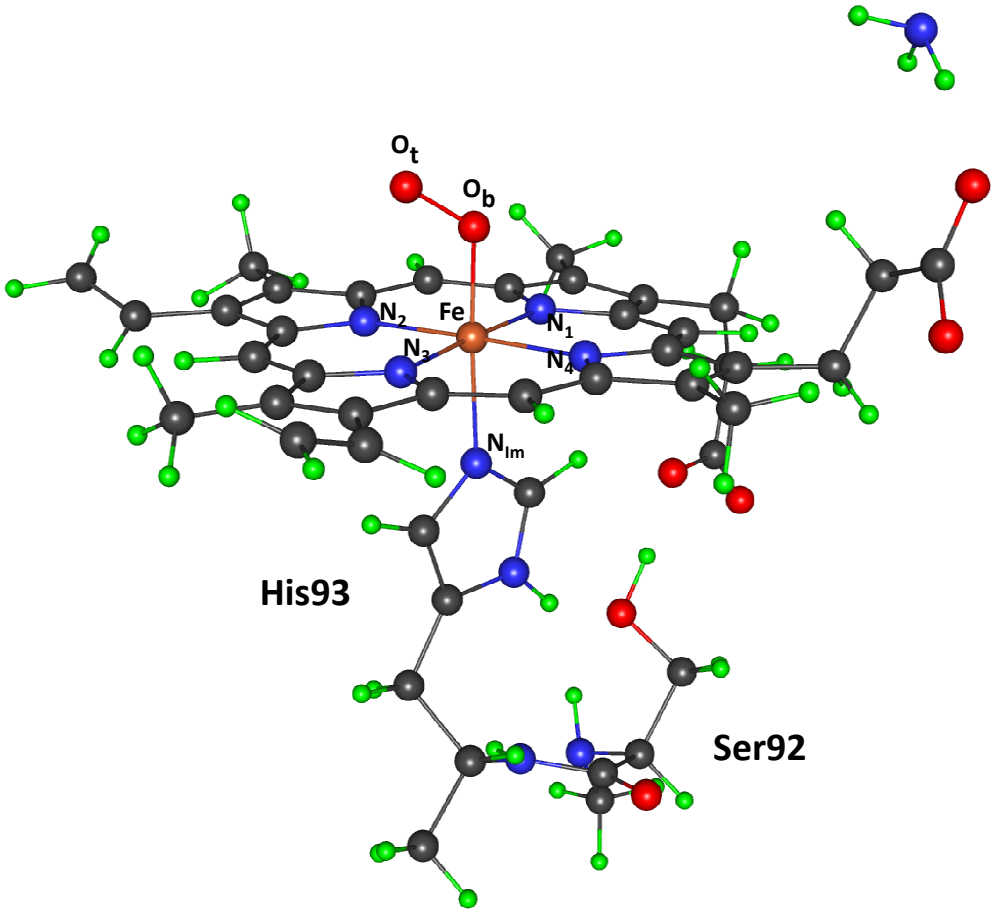

Figure S3: Structural model for the MbO_2 heme site optimized using DFT. Inclusion of the hydrogen bonding network stabilizes the observed His93 orientation. Color scheme: brown for iron, gray for carbon, blue for nitrogen, red for oxygen and green for hydrogen. Table S3 lists selected geometric parameters.

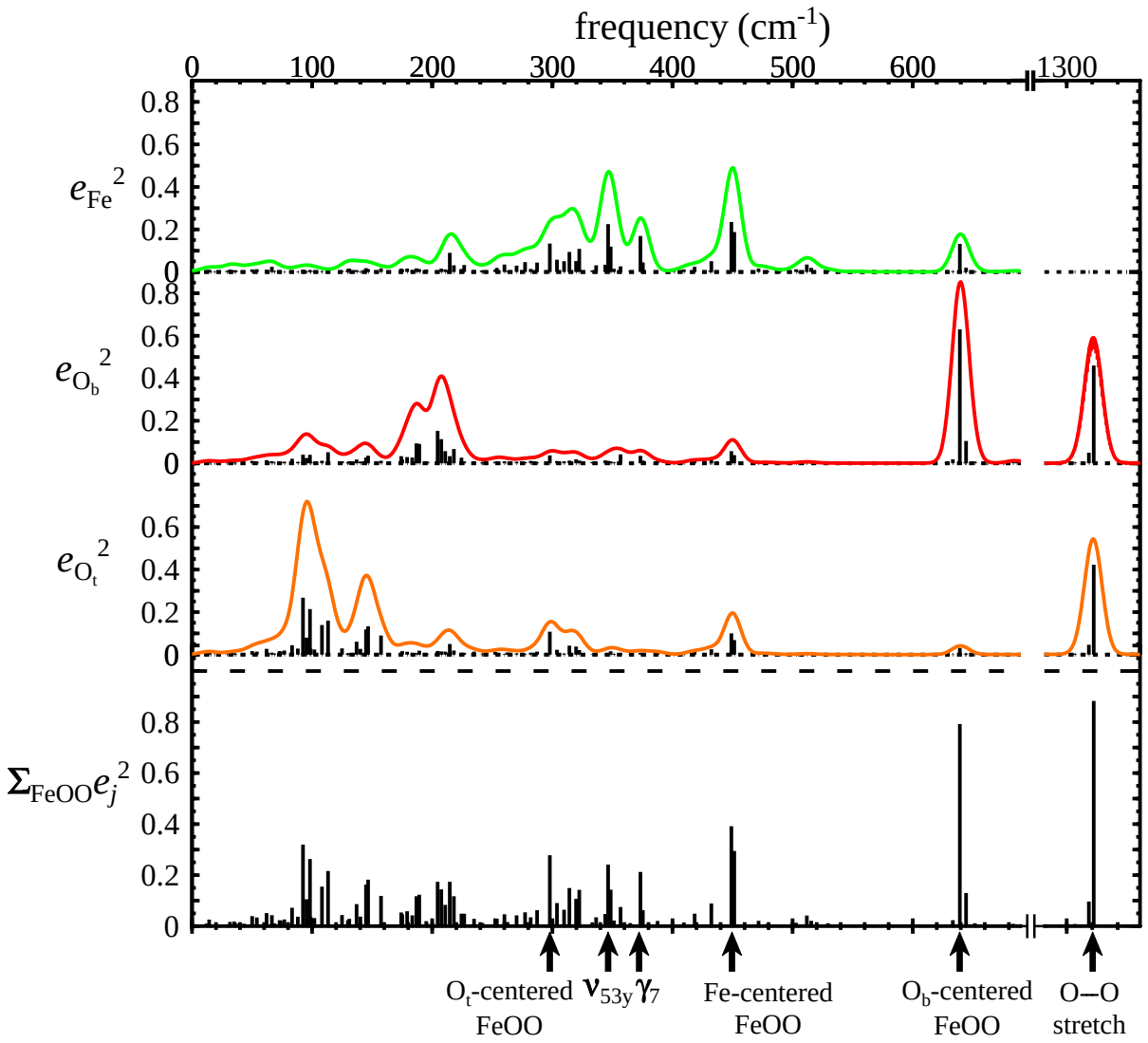

Figure S4: Calculated mode composition factors for Fe, the bound oxygen O_b, and the terminal oxygen O_t describe the kinetic energy distribution (KED) over the FeOO fragment for each vibrational mode of the MbO_2 model. The sum shown in the lower panel indicates the degree to which vibrational energy is localized on the three-atom fragment. Alternate version shown in Fig. S5.

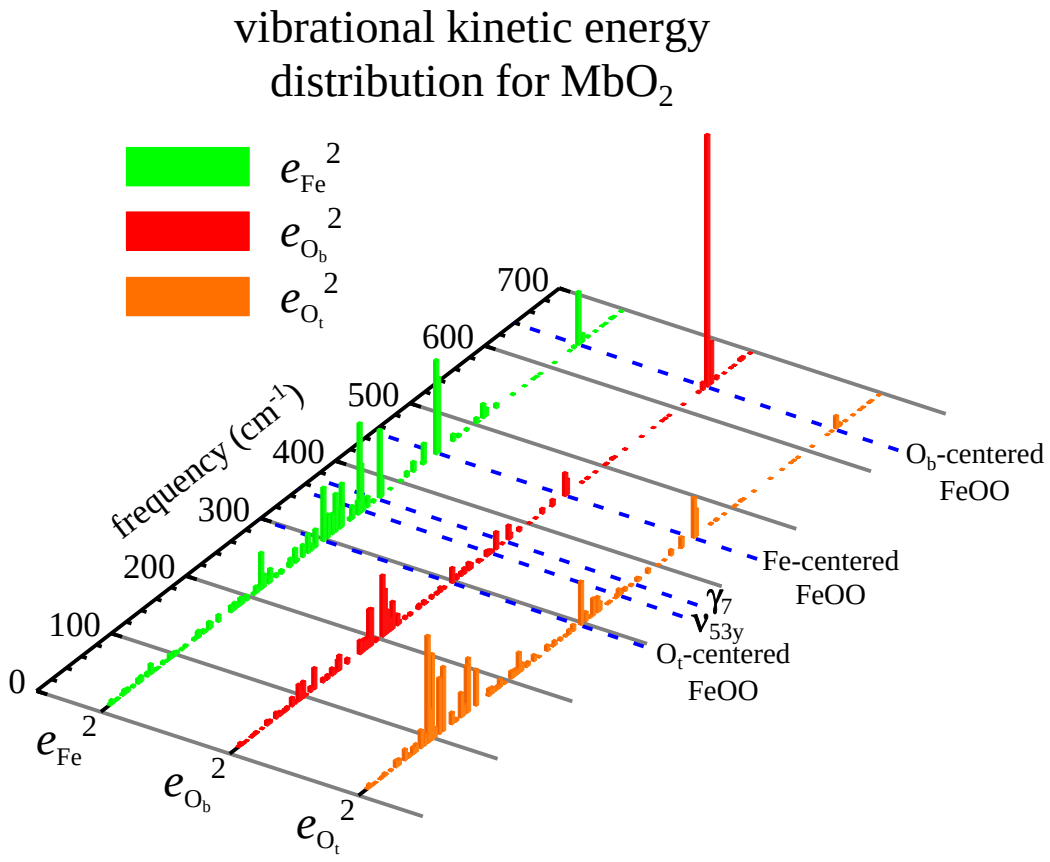

Figure S5: Alternate version of Fig. S4.

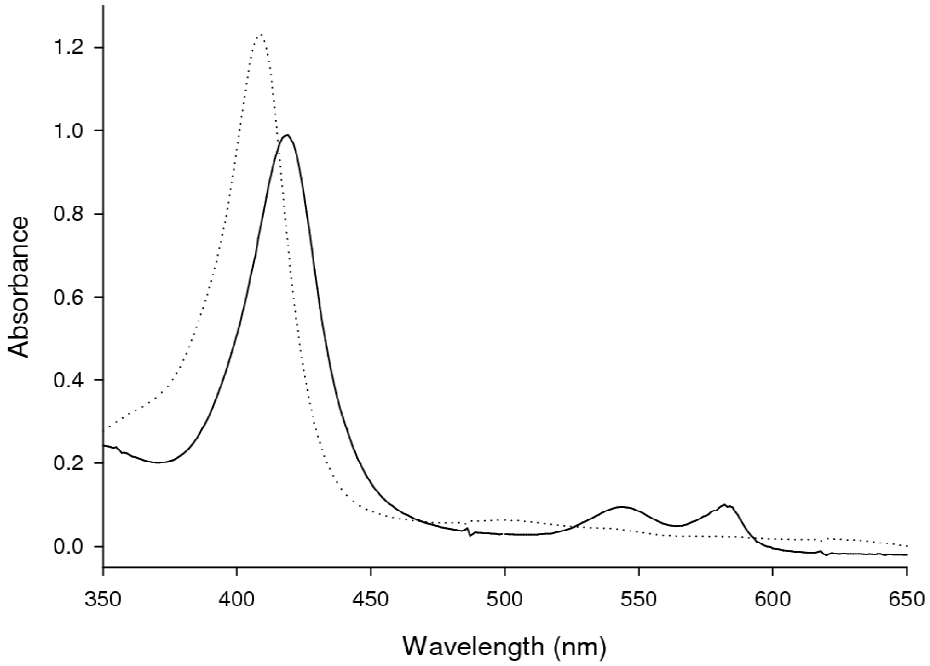

Figure S6: Electronic absorption spectrum of the ^{57}Fe-enriched Ag(I)−$Cu_B$$MbO_2$ NRVS sample. Solid line: Ag(I)−$Cu_B$$MbO_2$ diluted (1:1000) in 20 mM Mops buffer at pH 8.0. Dotted line: the same sample oxidized by 10 μM ferricyanide.

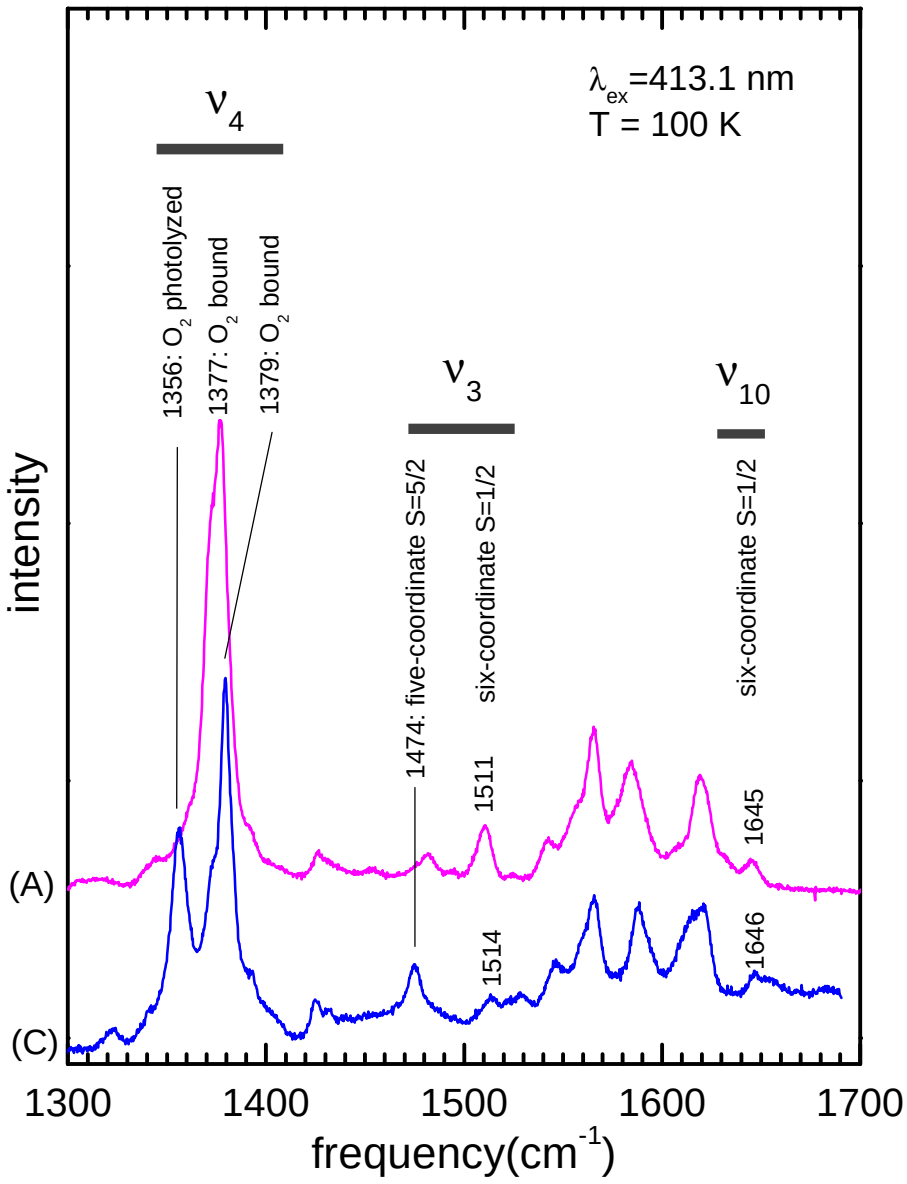

Figure S7: High frequency Raman spectra of (A) Ag(I)–$Cu_B MbO_2$ and (C) ^{54}Fe-enriched horse MbO_2, recorded at 100 K with 413.1 nm excitation, indicating ν_4, ν_3, ν_{10} frequencies diagnostic for the spin and coordination of the heme Fe. The presence of signals characteristic of five-coordinate high-spin heme reflect partial photolysis of the O_2 ligand from MbO_2.

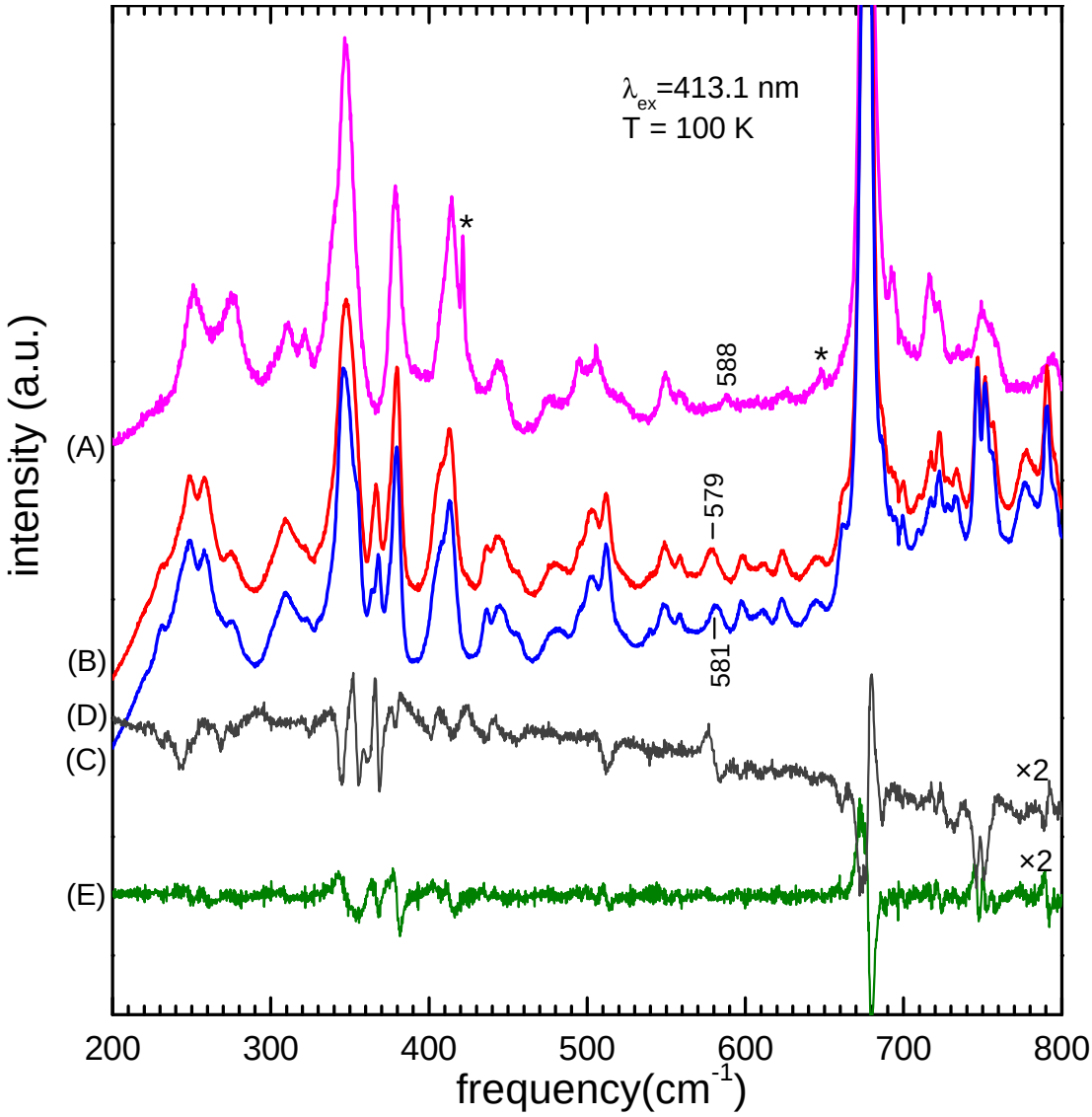

Figure S8: Raman spectra of Ag(I)−$Cu_B$$MbO_2$ (trace A) and horse MbO_2, recorded at 100 K using 413.1 nm excitation. Trace B:^{57}Fe-enriched MbO_2, trace C: ^{54}Fe-enriched MbO_2, trace D: difference between B and C. Trace E is obtained by shifting trace B to lower frequency by 0.3 cm^{-1} and subtracting the original spectrum, providing a reference that excludes significant grating drift [31]. Asterisks denote sharp lines at 421 and 648 cm^{-1} in the Ag(I)-CuBMbO_2 spectrum that result from Raman scattering from a sapphire window mounted on the back of the NRVS cell to allow direct excitation and collection of laser scattering from the sample.

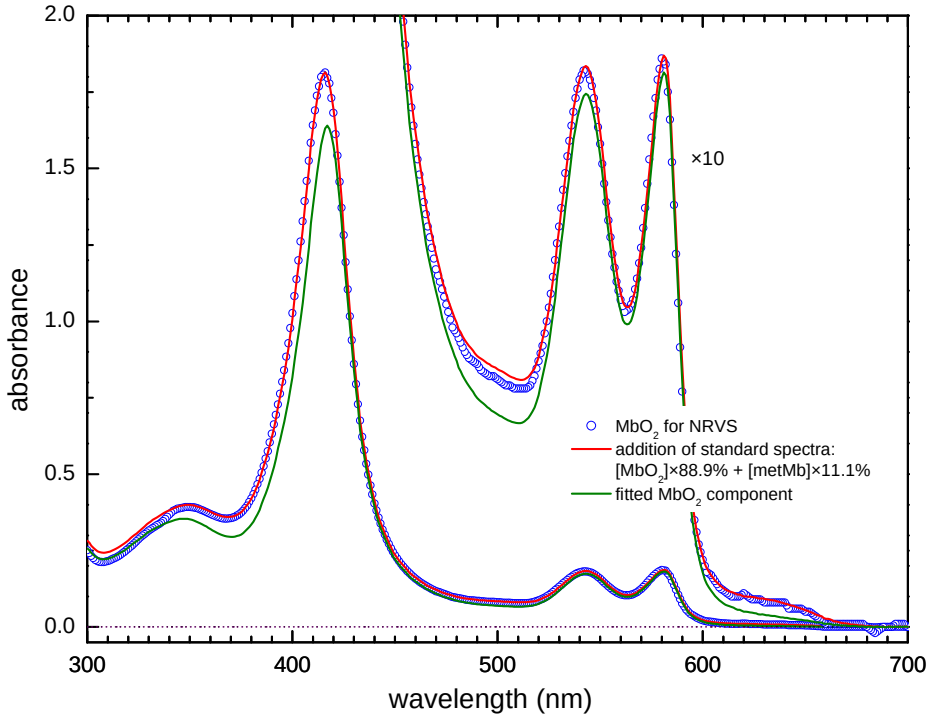

Figure S9: Electronic absorption spectrum of the horse MbO_2 NRVS sample. 3μL of the concentrated protein solution was diluted in 297 μL mother buffer for this measurement (blue circles). Optical path length is 1 mm. Standard spectra of horse MbO_2 and metMb were fit to the spectrum to determine their relative contributions in the NRVS sample.

References

[1] Teale, F. W. J. (1959) *Biochim. Biophys. Acta* **35**, 543

[2] Yonetani, T. (1967) *J. Biol. Chem.* **242**, 5008–5013

[3] Cho, B. M., Walker, R. C., Amer, H., Mercer, I., Klug, D. R., and Gould, I. R. (2005) *J. Phys. Chem. B* **109**, 5954–5961

[4] Rwere, F., Mak, P. J., and Kincaid, J. R. (2008) *Biochemistry* **47**, 12869–12877

[5] Sigman, J. A., Kwok, B. C., and Lu, Y. (2000) *J. Am. Chem. Soc.* **122**, 8192–8196

[6] Wang, N., Zhao, X., and Lu, Y. (2005) *J. Am. Chem. Soc.* **127**, 16541–16547

[7] Yu, N.-T. and Srivastava, R. B. (1980) *J. Raman Spectrosc.* **9**, 166–171

[8] Hu, S., Smith, K. M., and Spiro, T. G. (1996) *J. Am. Chem. Soc.* **118**, 12638–12646

[9] Sturhahn, W. (2004) *J. Phys.: Condens. Matter* **16**, S497–S530

[10] Zeng, W., Silvernail, N. J., Scheidt, W. R., and Sage, J. T. Nuclear resonance vibrational spectroscopy (NRVS). In *Application of Physical Methods to Inorganic and Bioinorganic Chemistry*, Ed. by Scott R. A. and Lukehart C. M., John Wiley & Sons, Ltd., (2007), pp401–421

[11] Toellner, T. S. (2000) *Hyperfine Interact.* **125**, 3–28

[12] Sturhahn, W. (2000) *Hyperfine Interact.* **125**, 149–172

[13] Lipkin, H. J. (1962) *Annals of Physics* **18**, 182 – 197

[14] Sturhahn, W., Toellner, T. S., Alp, E. E., Zhang, X., Ando, M., Yoda, Y., Kikuta, S., Seto, M., Kimball, C. W., and Dabrowski, B. (1995) *Phys. Rev. Lett.* **74**, 3832–3835

[15] Chumakov, A. I., Rüffer, R., Leupold, O., and Sergueev, I. (2003) *Struct. Chem.* **14**, 109–119

[16] Lipkin, H. J. (1995) *Phys. Rev. B* **52**, 10073–10079

[17] Adams, K. L., Tsoi, S., Yan, J., Durbin, S. M., Ramdas, A. K., Cramer, W. A., Sturhahn, W., Alp, E. E., and Schulz, C. (2006) *J. Phys. Chem. B* **110**, 530–536

[18] Leu, B. M., Ching, T. H., Zhao, J., Sturhahn, W., Alp, E. E., and Sage, J. T. (2009) *J. Phys. Chem. B* **113**, 2193–2200

[19] Frisch, M. J., Trucks, G. W., Schlegel, H. B., Scuseria, G. E., Robb, M. A., Cheeseman, J. R., Montgomery, J. A., Jr., Vreven, T., Kudin, K. N., Burant, J. C., Millam, J. M., Iyengar, S. S., Tomasi, J., Barone, V., Mennucci, B., Cossi, M., Scalmani, G., Rega, N., Petersson, G. A., Nakatsuji, H., Hada, M., Ehara, M., Toyota, K., Fukuda, R., Hasegawa, J., Ishida, M., Nakajima, T., Honda, Y., Kitao, O., Nakai, H., Klene, M., Li, X., Knox, J. E., Hratchian, H. P., Cross, J. B., Bakken, V., Adamo, C., Jaramillo, J., Gomperts, R., Stratmann, R. E., Yazyev, O., Austin, A. J., Cammi, R., Pomelli, C., Ochterski, J. W., Ayala, P. Y., Morokuma, K., Voth, G. A., Salvador, P., Dannenberg, J. J., Zakrzewski, V. G., Dapprich, S., Daniels, A. D., Strain, M. C., Farkas, O., Malick, D. K., Rabuck, A. D., Raghavachari, K., Foresman, J. B., Ortiz, J. V., Cui, Q., Baboul, A. G., Clifford, S., Cioslowski, J., Stefanov, B. B., Liu, G., Liashenko, A., Piskorz, P., Komaromi, I., Martin, R. L., Fox, D. J., Keith,

T., Al-Laham, M. A., Peng, C. Y., Nanayakkara, A., Challacombe, M., Gill, P. M. W., Johnson, B., Chen, W., Wong, M. W., Gonzalez, C., and Pople, J. A. *Gaussian 03, Revision D.01*. Gaussian, Inc., Wallingford, CT, 2004

[20] Becke, A. D. (1993) *J. Chem. Phys.* **98**, 5648–5652

[21] Lee, C., Yang, W., and Parr, R. G. (1988) *Phys. Rev. B* **37**, 785–789

[22] Schäfer, A., Horn, H., and Ahlrichs, R. (1992) *J. Chem. Phys.* **97**, 2571–2577

[23] Leu, B. M., Zgierski, M. Z., Wyllie, G. R. A., Scheidt, W. R., Sturhahn, W., Alp, E. E., Durbin, S. M., and Sage, J. T. (2004) *J. Am. Chem. Soc.* **126**, 4211–4227

[24] Barabanschikov, A., Demidov, A., Kubo, M., Champion, P. M., Sage, J. T., Zhao, J., Sturhahn, W., and Alp, E. E. (2011) *J Chem Phys* **135**, 015101

[25] Chen, H., Ikeda-Saito, M., and Shaik, S. (2008) *J. Am. Chem. Soc.* **130**, 14778–14790

[26] Li, J., Peng, Q., Barabanschikov, A., Pavlik, J. W., Alp, E. E., Sturhahn, W., Zhao, J., Schulz, C. E., Sage, J. T., and Scheidt, W. R. (2011) *Chemistry* **17**, 11178–11185

[27] Sage, J. T., Paxson, C., Wyllie, G. R. A., Sturhahn, W., Durbin, S. M., Champion, P. M., Alp, E. E., and Scheidt, W. R. (2001) *J. Phys.: Condens. Matter* **13**, 7707–7722

[28] Pavlik, J. W., Barabanschikov, A., Oliver, A. G., Alp, E. E., Sturhahn, W., Zhao, J., Sage, J. T., and Scheidt, W. R. (2010) *Angew. Chem. Int. Ed.* **49**, 4440–4404

[29] Hirota, S., Ogura, T., Appelman, E. H., Shinzawah-Itoh, K., Yoshikawa, S., and Kitagawa, T. (1994) *J. Am. Chem. Soc.* **116**, 10564–10570

[30] Jeyarajah, S., Proniewicz, L. M., Bronder, H., and Kincaid, J. R. (1994) *J. Biol. Chem.* **269**, 31047–31050

[31] Takahashi, S., Ishikawa, K., Takeuchi, N., Ikeda-Saito, M., Yoshida, T., and Rousseau, D. L. (1995) *J. Am. Chem. Soc.* **117**, 6002–6006

[32] Hirota, S., Li, T., Phillips, G. N., Jr., Olson, J. S., Mukai, M., and Kitagawa, T. (1996) *J. Am. Chem. Soc.* **118**, 7845–7846

[33] Nicoletti, F. P., Thompson, M. K., Franzen, S., and Smulevich, G. (2011) *J. Biol. Inorg. Chem.* **16**, 611–619

[34] Garton, E. M., Pixton, D. A., Petersen, C. A., Eady, R. R., Hasnain, S. S., and Andrew, C. R. (2012) *J. Am. Chem. Soc.* **134**, 1461–1463

[35] Yanagisawa, S., Yotsuya, K., Hashiwaki, Y., Horitani, M., Sugimoto, H., Shiro, Y., Appelman, E. H., and Ogura, T. (2010) *Chem. Lett.* **39**, 36–37

[36] Tomita, T., Gonzalez, G., Chang, A. L., Ikeda-Saito, M., and Gilles-Gonzalez, M.-A. (2002) *Biochemistry* **41**, 4819–4826

[37] Karow, D. S., Pan, D., Tran, R., Pellicena, P., Presley, A., Mathies, R. A., and Marletta, M. A. (2004) *Biochemistry* **43**, 10203–10211

[38] Avila, L., Huang, H.-W., Rodríguez, J. C., Moënne-Loccoz, P., and Rivera, M. (2000) *J. Am. Chem. Soc.* **122**, 7618–7619

[39] Yukl, E. T., Ioanoviciu, A., de Montellano, P. R. O., and Monne-Loccoz, P. (2007) *Biochemistry* **46**, 9728–9736

[40] Das, T. K., Weber, R. E., Dewilde, S., Wittenberg, J. B., Wittenberg, B. A., Yamauchi, K., Hauwaert, M. L. V., Moens, L., and Rousseau, D. L. (2000) *Biochemistry* **39**, 14330–14340

[41] Aono, S., Kato, T., Matsuki, M., Nakajima, H., Ohta, T., Uchida, T., and Kitagawa, T. (2002) *J. Biol. Chem.* **277**, 13528–13538

[42] Yeh, S. R., Couture, M., Ouellet, Y., Guertin, M., and Rousseau, D. L. (2000) *J. Biol. Chem.* **275**, 1679–1684

[43] Mukai, M., Savard, P.-Y., Ouellet, H., Guertin, M., and Yeh, S.-R. (2002) *Biochemistry* **41**, 3897–3905

[44] Das, T. K., Couture, M., Ouellet, Y., Guertin, M., and Rousseau, D. L. (2001) *Proc. Natl. Acad. Sci. U S A* **98**, 479–484

[45] Lu, C., Egawa, T., Wainwright, L. M., Poole, R. K., and Yeh, S.-R. (2007) *J. Biol. Chem.* **282**, 13627–13636

[46] Macdonald, I. D. G., Sligar, S. G., Christian, J. F., Unno, M., and Champion, P. M. (1999) *J. Am. Chem. Soc.* **121**, 376–380

[47] Thompson, H., Yu, N., and Gersonde, K. (1987) *Biophy. J.* **51**, 289 – 295

[48] Chartier, F. J. M., Blais, S. P., and Couture, M. (2006) *J. Biol. Chem.* **281**, 9953–9962

[49] Zeng, W., Silvernail, N., Wharton, D. C., Georgiev, G. Y., Leu, B. M., Scheidt, W. R., Zhao, J., Sturhahn, W., Alp, E. E., and Sage, J. T. (2005) *J. Am. Chem. Soc.* **127**, 11200–11201

[50] Unno, M., Chen, H., Kusama, S., Shaik, S., and Ikeda-Saito, M. (2007) *J Am Chem Soc* **129**, 13394–13395

[51] Vojtechovský, J., Chu, K., Berendzen, J., Sweet, R. M., and Schlichting, I. (1999) *Biophys J* **77**, 2153–2174

[52] Sigman, J. A., Kim, H. K., Zhao, X., Carey, J. R., and Lu, Y. (2003) *Proc Natl Acad Sci USA* **100**, 3629–3634